IMEKO International Conference on
Metrology for Archaeology and Cultural Heritage
Lecce, Italy, October 23-25, 2017

Shifting Zoom on a Linear Inverse Scattering Algorithm Applied to GPR Data

Raffaele Persico[1,2], Giovanni Ludeno[3], Francesco Soldovieri[3], Albéric De Coster[4], Sébastien Lambot[4]

[1] *Institute for Archaeological and Monumental Heritage IBAM-CNR, Lecce, Italy, r.persico@ibam.cnr.it*
[2] *International Telematic University Uninettuno UTIU, Rome, Italy*
[3] *Institute for the Electromagnetic Sensing of the Environment IREA-CNR, Naples, Italy, ludeno.g@irea.cnr.it, soldovieri.f@irea.cnr.it*
[4] *Université Catholique de Louvain, Louvain-la-Neuve, Belgium, sebastien.lambot@uclouvain.be, alberic.decoster@uclouvain.be*

***Abstract* – In this contribution a shifting zoom on GPR data is applied for the reconstruction of buried targets in the framework of a linear inverse scattering algorithm, and in particular the improvement of the image achieved on depth slices is put into evidence. Shifting zoom is a way to mitigate the problem of the limited view, which is particularly relevant in inverse scattering algorithms since the computational burden related to the calculation and the inversion of large matrixes compels to limit the inversion to investigation domains not very large in terms of wavelength. The dealing will be back-upped with an experimental validation.**

I. INTRODUCTION

Inverse scattering applied to GPR data has been an issue of interest for many years now. The reconstruction of the buried targets is often recast as a linearized inverse problem where the unknown quantity is the difference of permittivity (possibly complex in order to account also for the conductivity) between the targets and the surrounding soil [1-3] or the identification of equivalent buried sources of field that are supported in the volume occupied by the buried targets, which is more probably called an inverse source approach [4]. The linearization is often based on a Born model, even if other possibilities exist [5-6]. It has been shown that a Born model is in general able to provide a satisfying reconstruction of the shape of the targets , even in cases quite beyond the limits of the Born Approximation [7], but fails in the quantitative reconstruction of the unknown looked for. Moreover, a linear model is computationally quite less demanding than a nonlinear one and is immune from the problem of false solutions that might trap the minimization of the relevant cost functional [8]. Even so, linear inversion algorithms are in general computationally demanding when the area to be investigated is electrically large, which is virtually all the times the case in GPR prospecting. So, further approximations have been introduced in order to reduce to a minimum the needed computational time and also the RAM memory needed to perform the inversion. In particular, migration algorithms, that can be recast either as a sort of inverse source approach [9-10] or as an inverse scattering approach [2], and are essentially based on the approximation of the relevant inverse operator with the corresponding adjoint operator. The adjoint operator is easily calculated numerically when the operator is discretized into a matrix because, as well known, it corresponds to the conjugate transposed matrix. However, in general formulation a discretization in order to perform the migration is not needed either, because integral formulas (even if approximated) providing the result in closed form are available [2, 9-10].

So, at the end we can distinguish a migration from a properly said linear inversion, where for linear inversion we mean an inversion where the problem is discretized and the relevant matrix is numerically inverted (the problem is not resoluble in a closed form, at least with reference to the case of commonly meant GPR data). The inversion is meant regularized [11], being the problem at hand ill posed [2].

In general, a migration can be applied without problems to a large investigation domain, as large as several hundredths square wavelengths, and is inserted ad an automatic routine in the most common commercial codes for the processing of GPR data, as the reflex and the GPR Slices. A linear inversion algorithm, instead, is in general applicable on a domain only long and deep a few wavelengths, let say of the order of a few tens at most if the available computer is very performing.

In this paper we afford exactly this problem, and propose a way through which a long investigation domain can be reconstructed making use of a linear inversion algorithm.

This is done by dividing in subparts the investigation domain, and combining suitably the achieved partial results, in a way that avoids some problems related to the simple sequential addition of subsequent adjacent reconstructions.

II. FORMULATION OF THE PROBLEM

Under a Born model, a linear integral relationship relates the electric scattered field E_s generated by any buried anomaly (the reference situation is a homogeneous soil) to the unknown dielectric contrast χ, that is the relative difference between the (possibly complex) dielectric permittivity of the buried anomalies and that of the surrounding soil. This relationship is given by:

$$E_s(\mathbf{r}_o,\omega) = k_b^2 \iint_{\Lambda} G(\mathbf{r}_o - \mathbf{r}',\omega) E_{inc}(\mathbf{r}_o,\mathbf{r}',\omega)\chi(\mathbf{r}')d\mathbf{r}' \quad (1)$$

In eq. 1, G is the Green′s function, E_{inc} is the incident field and k_b is the wave number in the reference homogeneous medium. A multi-monostatic measurement configuration is meant. The incident field is modeled as the field generated by a unitary filamentary current placed at $\mathbf{r}_o$. The subscript "$_O$" denotes the observation point, belonging to the observation domain. Λ is the investigation domain, i.e., the spatial region where the targets are assumed to reside.

Here we will make use of a homogeneous reference scenario, which makes both incident field and Green's function proportional to a Hankel function $H_0^{(2)}(\cdot)$ [12] of second kind and zero order. Consequently, eq. (1) is particularized into:

$$E_s(\mathbf{r}_o,\omega) = j\frac{\omega\mu_0}{8} k_b^2 \iint_{\Lambda} \left[H_0^{(2)}\left(k_b|\mathbf{r}_o - \mathbf{r}'|\right)\right]^2 \chi(\mathbf{r}')d\mathbf{r}' \quad (2)$$

The right hand side of eq. (2) quantifies the linear operator $\boldsymbol{L}$ relating the unknown contrast function to the scattered field data. This linear integral operator $\boldsymbol{L}$ can be expressed in terms of its Singular Value Decomposition (SVD) [11]. Specifically, if σ_n is the n-th singular value, $\boldsymbol{v}_n$ and $\boldsymbol{u}_n$ are the n^{th} left and right singular function, respectively, then the solution of the inverse scattering problem is provided by [11-12]:

$$\boldsymbol{\chi}(\mathbf{r}) = \sum_{n=1}^{\infty} \frac{1}{\sigma_n} \langle \mathbf{E}_s, \mathbf{u}_n \rangle \mathbf{v}_n(\mathbf{r}) \quad \mathbf{r} \in \Lambda \quad (3)$$

However, the ill-posedness of the problem compels to adopt some regularization. One of the classical regularization schemes is the Truncated SVD (TSVD), where the solution is provided by:

$$\hat{\boldsymbol{\chi}}(\mathbf{r}) = \sum_{n=1}^{T} \frac{1}{\sigma_n} \langle \mathbf{E}_s, \mathbf{u}_n \rangle \mathbf{v}_n(\mathbf{r}) \quad \mathbf{r} \in \Lambda \quad (4)$$

We also will make use of a TSDV. The choice of T is a compromise between accuracy and robustness of the solution. In practical cases, it is probably well advised to try different values of T and choose heuristically that that provides the apparently clearer solution. This is the way that we will follow, even if we will show only the results achieved with the heuristically best threshold. In particular, analytical evaluations of the best threshold exist [11] too, but they are based on the amount of noise in the data, which in the field is not easily measurable, at least with a conventional GPR system.

III. THE SHIFTING ZOOM

Let now show what is the shifting zoom. As said, a long investigation domain in general cannot be "inverted" making use af a unique global discretized operator. Consequently, in order to invert a long investigation domain, the most natural choice is to adopt subsequent adjacent investigation domains along the radar profile, and consequently to adopt subsequent observation lines superposed to ech of the adjacent investigation domains, according to a scheme indicated in Fig. 1. However, this introduces a problem of limited view angle for the targets peripheral with respect to the "current" investigation domain where they are placed. For example, target ***c*** in Fig. 1 is peripheral with respect to the observation line L_2. Moreover, a target as the object ***a*** might cause artefacts in the investigation domain D_2, because it is quite probably perceived by the antennas when they pass on the left edge of L_2. Of course, the problem of the peripheral targets (that are seen under a reduced and asymmetric comprehensive maximum view angle) and the problem of the external targets that might create artefacts in the current investigation domains are two aspects of the same issue. For example, target ***a*** is also peripheral with respect to D_1 and target ***c*** is a possible source of artefacts in D_3. Of course, neither **a** nor **c** are targets peripheral with respect to the comprehensively gathered profile, and so the problem is arisen by the subdivision of the radar profile into adjacent investigation-observation domains. Please note that the proposed schematic encloses also the case of a target that crosses the edge between two adjacent domains: such an object, in fact, can be seen as a couple of adjacent targets, one on the left hand side and one on the right hand side of the edge.

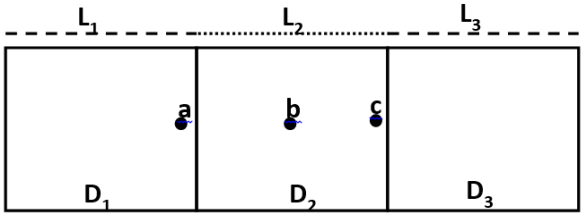

Fig. 1. Pictorial for an inversion of a long radar image making use of adjacent investigation-observation domains

Here, we propose to overcome the problem by means of suitably overlapped investigation-observation domains instead of adjacent ones, as described in Fig. 2. The method consists in retaining only the central belt of the reconstruction achieved for the current investigation domain.

The central belt is meant as follows: if the nth reconstruction result is provided by a matrix $A(i,j)$ of n x m pixels, the central belt is the central belt the column $A(i, (m + 1)/2)$, $i = 1…n$ if m is odd, and is the couple of central columns $A(i, (m/2))$ and $A(i, (m/2) + 1)$ if m is even.

After on, the subsequent investigation domain is shifted of the amount of this belt with respect to the previous one. In particular, in Fig. 2 the generic k^{th} investigation domain is indicated in red, and its central belt is coloured in red too. The homologous areas with respect to the $(k + 1)^{th}$ investigation domain are instead labelled in green. Also the observation lines have to be coherently shifted, so to keep them hanged on the relative underlying investigation domains, as shown in Fig. 2. This compel to adopt a size of the pixel and a spatial step of the data equal to each other or at least chosen with an integer ratio between them, in order to keep properly hanged the current investigation and observation domains. It is also needed that the last measurement point exploited for the n^{th} inversion is re-exploited as the first measurement point exploited for the $(n+1)^{th}$ inversion.

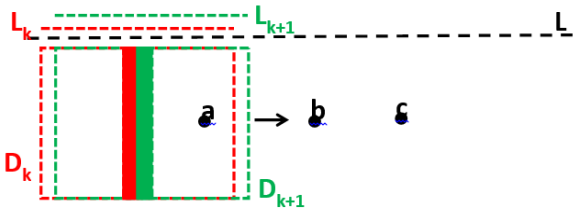

Fig. 2. Pictorial of the shifting zoom

When making use of a shifting zoom the joined reconstructions are relative to central belts of observation domains. Therefore, no peripheral target is artificially created. At the same time, the undesired effects of targets immediately external to the current observation-investigation domain are made negligible, because these targets are certainly distant from the central belt of that investigation domain and so their effect is negligible. Of course, the left side half of the first investigation domain (before the "first central belt") and the right side half of the last investigation domain (after the "last central belt") are joined too to the reconstruction, in order not too loose the information contained in these data.

IV. EXPERIMENTAL RESULTS

The exploited GPR system was a vector network analyzer (VNA), which constituted a stepped-frequency continuous-wave (SFCW) radar system (ZVRE, Rohde & Schwarz, Munich, Germany) and a linearly polarized, double-ridged broadband horn antenna (BBHA 9120 A, Schwarzbeck Mess-Elektronik, Schönau, Germany) as simultaneous transmitter and receiver. The antenna nominal frequency band ranges from 0.8 to 5.0 GHz and its isotropic gain ranges from 6 to 18 dBi. The relatively high directivity of the antenna (45° −3 dB beam width in the E-plane and 30° in the H-plane at 1 GHz) makes it immune to interferences from external sources or reflectors, which enforces the homogeneous space reference model. The antenna was connected to the reflection port of the VNA via a high quality N-type 50-Ohm coaxial cable.

The calibration of the VNA at the connection between the antenna feed point and the cable was achieved using an Open-Short-Match calibration kit. After that, data were gathered at 1601 frequencies equally spaced (Δf=2MHz) between 800 and 4000 MHz.

The radar measurements were performed over a 3 × 3 m dry sand box with the antenna aperture at height 1 cm above the sand. A copper sheet assumed as a perfect electrical conductor (PEC) was installed at the bottom of the 0.86 m thick sand layer to control the boundary conditions. The targets were three PVC pipes of 1.20 m length and 50 mm diameter with a thickness of 1.8 mm and were buried at 0.07, 0.29, and 0.51 m depth, respectively. The three pipes were displaced about parallel to each other, and their horizontal distance from the start point of the Bscans were about equal to 047, 1.17 and 1.97 m, respectively. The pipes were filled with air. The radar system was installed on a XYZ automated positioning table to automatically acquire the data over a 2.40 m long profile with a position step of 1 cm. The radar profiles was transversal with respect to the pipes.

Following the near-field radar antenna model of Lambot and André [13], the antenna global reflection and transmission functions were determined. Then, in order to remove a part of the antenna effects, the free-space response of the antenna was subtracted from $S_{11}(f)$. The frequency-domain radar data were subsequently converted into the time domain using the inverse Fourier Transform and a zero timing together with a background removal were subsequently applied to highlight the targets.

We have gathered comprehensively 49 Bscans, each of which 240 cm long, with interline space of 5 cm. The measurement step was 1 cm along each Bscan. Then we have performed a virtual shift of the data of 35 cm, eliminating the first data and zero padding after the end of the Bscans. In this way, we have that the three targets are at 12, 82 and 162 cm. Then we have inverted the data making use of three adjacent investigation-observation domains, each of which 80 cm long. The adopted data-

shift and subdivision makes peripheral all the involved pipes. For the inversion, a relative permittivity equal to 2.37 (on the basis of the diffraction hyperbolas [14]) has been adopted, and the TSVD has been regularized stopping the summation of eq. (4) up to the last singular value higher or equal to -30 dB with respect to the first one. Three depth slices (at the depth levels of the pipes) achieved making use of three adjacent investigation-observation domains, each of which 80 cm large, are shown in Fig. 3. The homologous slices achieved with a shifting zoom are shown in Fig. 4. As can be seen, in Fig. 4 we don't have seam effects and the three pipes are cleaner than in Fig. 3, where the reconstruction of the second and third pipe is weaker and more blurred due to the fact that these targets are placed between two adjacent investigation domains. The extra anomalies beyond the three pipes are probably due to some metallic impureness present in the test tank.

V. CONCLUSIONS

In the present contribution, a shifting zoom procedure has been proposed for the numerical linear inversion of possibly electrically large investigation domains in the framework of GPR prospecting. We have shown experimental data gathered in a controlled situation and have shown in particular the effect of a shifting zoom on depth slices highlighting the presence of three pipes.

In a future, the procedure will be tested on data gathered in the field.

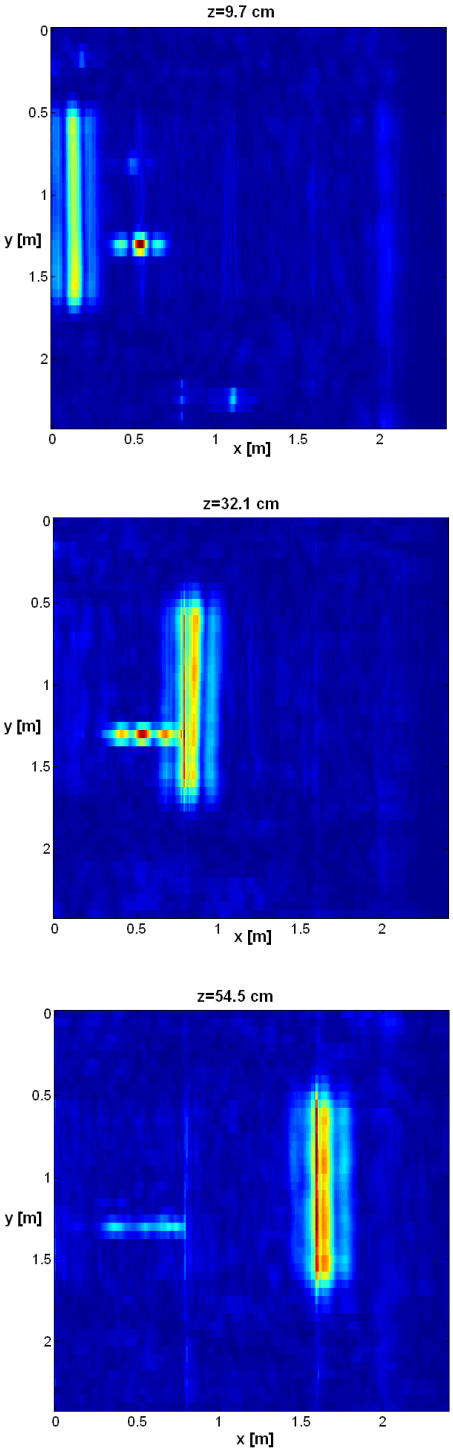

Fig. 3. From top to bottom: depth slices centered at depth levels 9.7, 32.1 and 54.5 respectively. The slices are adjacent observation domains

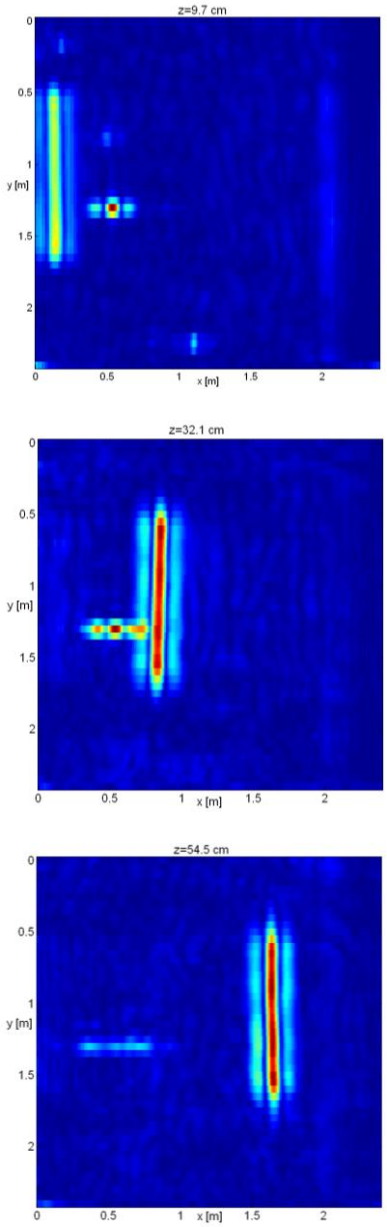

Fig. 4. From top to bottom: depth slices centered at depth levels 9.7, 32.1 and 54.5 respectively. The slices are achieved with a shifting zoom

REFERENCES

[1] D. Lesselier, B. Duchene, Wavefield inversion of objects in stratified environments: from back-propagation schemes to full solutions, in Review of Radio Science 1993-1996, ed. R. Stone, Oxford University press, 1996.

[2] R. Persico, Introduction to Ground Penetrating Radar: Inverse Scattering and data processing. Wiley, 2014, ISBN 9781118305003.

[3] D. Colton, R. Kress, Integral Equation Methods in Scattering Theory, SIAM, 2013, ISBN: 978-1-61197-315-0

[4] A. J. Devaney, Inverse Source and Scattering Problems in Ultrasonics, IEEE Trans. on Sonics and Ultrasonics, vol. SU-30, n. 6, pp. 355-364, 1983.

[5] L. Manica, P. Rocca, M. Salucci, M. Carlin and A. Massa,Scattering Data Inversion Through Interval Analysis Under Rytov Approximation, Proc. of 7th European Conference on Antennas and Propagation, Gothenburg, Sweden, 8-11 April 2013

[6] A. Liseno, F. Tartaglione, F. Soldovieri, "Shape reconstruction of 2d buried objects under a Kirchhoff approximation", **IEEE Geoscience and Remote Sensing Letters,** vol.1, no. 2, pp.118-121, 2004.

[7] F. Soldovieri, R. Persico, "Reconstruction of an embedded slab from multifrequency data under the distorted Born approximation", *IEEE. Trans. On Antennas and Prop*., vol. 52, n. 9, pp. 2348-2356, September 2004.

[8] R. Persico, F. Soldovieri, R. Pierri, "Convergence Properties of a Quadratic Approach to the Inverse Scattering Problem", *Journal of Optical Society of America Part A*, vol. 19, n. 12, pp. 2424-2428, December 2002.

[9] R. H. Stolt, Migration by Fourier Transform, Geophysics, vol. 43, n. 1, pp. 23-48, 1978.

[10] W. A. Schneider, Integral formulation for migration in two and three dimensions, Geophysics, vol. 43, n. 1, pp. 49-76, 1978.

[11] M. Bertero and P. Boccacci, Introduction to Inverse Problems in Imaging, Institute of Physics Publishing, Bristol and Philadelphia, 1998.

[12] Persico, R.; Pochanin, G.; Ruban, V.; Orlenko, A.; Catapano, I.; Soldovieri, F. Performances of a Microwave Tomographic Algorithm for GPR Systems Working in Differential Configuration. *IEEE J. Sel. Topics Appl. Earth Observ. Remote Sens.* 2016, 9, 1343–1356. doi:10.1109/JSTARS.2015.2489720.

[13] Lambot, S.; André, F. Full-Wave Modeling of Near-Field Radar Data for Planar Layered Media Reconstruction. *IEEE Trans. Geosci. Remote Sens.* 2014, *52*, 2295–2303.

[14] L. Mertens_, R. Persico, L. Matera, S. Lambot, Smart automated detection of reflection hyperbolas in complex GPR images With No A Priori Knowledge on the Medium, IEEE Transaction on Geosciences and Remote Sensing, vol. 54, n. 1, pp. 580-596, doi **10.1109/TGRS.2015.2462727**, 2016